Robust Predictive Current Control With Online Disturbance Estimation for Induction Machine Drives

Bo Wang, *Student Member, IEEE*, Xianle Chen, Yong Yu, Gaolin Wang, *Member, IEEE*, and Dianguo Xu, *Senior Member, IEEE*

***Abstract*—This paper presents robust predictive current control (RPCC) with online disturbance estimation to achieve high-performance current loop for induction machine (IM) drives. The disturbance caused by parameter variations and other unmodeled dynamics is considered in modeling of IM. Based on this model, the control law of the proposed scheme is derived, where a discrete Luenberger observer is designed to estimate the future values of stator current and disturbance. The selection of the designed observer gain is a compromise between the system control bandwidth and robustness. Compared with the conventional RPCC, the proposed scheme removes the steady-state current error caused by the system disturbance. Experimental results on an industrial induction machine drive show that the proposed scheme provides fast and static-errorless current tracking even with mismatched machine parameters.**

***Index Terms*—Discrete Luenberger observer, induction machine (IM) drives, online disturbance estimation, robust predictive current control (RPCC).**

NOMENCLATURE

R_s	Stator resistance.
R_r	Rotor resistance.
L_s	Stator inductance.
L_r	Rotor inductance.
L_m	Mutual inductance.
ω_e	Synchronous angular speed.
ω_r	Rotor angular speed.
λ_r	Rotor flux.
$\sigma = 1 - L_m^2/(L_s L_r)$	Leakage coefficient.
$\boldsymbol{u} = [u_{sd}\ u_{sq}]^T$	Stator voltage.
$\boldsymbol{i} = [i_{sd}\ i_{sq}]^T$	Stator current.
$\boldsymbol{d} = [d_{sd}\ d_{sq}]^T$	Back electromagnetic force (EMF).
$\boldsymbol{f} = [f_{sd}\ f_{sq}]^T$	Disturbances caused by parameter variations and other unmodeled dynamics uncertainties.
$\boldsymbol{\varepsilon} = [\varepsilon_d \varepsilon_q]^T$	Unmodeled dynamics uncertainties.
p	Differential operator.
Δ	Parameter uncertainties.
$\hat{\ }$	Estimated value.
$[]_{\mathrm{ref}}$	Reference value.
$[]_{\mathrm{d}}$, $[]_{\mathrm{q}}$	Quantities on the synchronous rotating dq reference frame.
$[]_{\alpha}$, $[]_{\beta}$	Quantities on the stationary $\alpha\beta$ reference frame.

Manuscript received March 25, 2016; revised June 21, 2016 and August 9, 2016; accepted August 21, 2016. Date of publication August 25, 2016; date of current version February 11, 2017. This work was supported by the National Natural Science Foundation of China (51377032). Recommended for publication by Associate Editor J. R. Rodriguez.

The authors are with the School of Electrical Engineering and Automation, Harbin Institute of Technology, Harbin 150001, China (e-mail: wangbo6222@126.com; chen_xianle@126.com; yuyong@hit.edu.cn; WGL818@hit.edu.cn; xudiang@hit.edu.cn).

Color versions of one or more of the figures in this paper are available online at http://ieeexplore.ieee.org.

Digital Object Identifier 10.1109/TPEL.2016.2602853

I. INTRODUCTION

INDUCTION machine (IM) drives based on indirect field-oriented control (IFOC) have been widely applied in industry due to the good speed-regulating performance [1]–[3]. In an IFOC-based IM drive, the double-loop structure is usually adopted. The outer loop (speed loop) adjusts the machine speed, while the inner loop (current loop) regulates the stator current to track its reference [4]. Thus, the speed and stability of the current loop are the key factors in the whole drive system.

In recent years, different schemes have been introduced into the current loop control, e.g., hysteresis-band control [5], proportional-integral (PI) control [6], proportional resonant control [7], complex vector control [8], and predictive current control [9]–[15]. In these control strategies, deadbeat-based predictive current control (DPCC) can calculate the required command voltage once every sampling period based on object model, and make feedback current optimally track its reference. Compared with the commonly-used PI control [6], DPCC achieves fast current response, which permits the increase of outer loop bandwidth [10], [11]. Therefore, DPCC has lately attracted attention of researchers, and has been used in different applications, e.g., three-phase inverter control [16], [17], permanent magnet synchronous motor drives [18].

Although DPCC has the advantage of fast current response, the controller instability always occurs [10]. This is because the conventional DPCC completely depends on object model, but in a practical control system, the parameter error of control object and other unmodeled dynamics would lead to model mismatch, which deteriorates the performance of DPCC. For IM drives, the machine parameters cannot remain constant under factors like magnetic saturation (inductances) and ambient temperature (resistances) [19], so the robustness of DPCC is a pivotal issue.

As analyzed in [20], the conventional DPCC is capable to tolerate a maximum inductance reduction of 50% of the nominal value and a maximum control delay of less than two sampling periods. To extend these limits, a modified DPCC, which is named robust predictive current control (RPCC), is presented in [20] and [21]. The RPCC combines the conventional DPCC with a Luenberger observer to estimate the future current values,

which reduces the controller dependence on object model and leads to improved robustness. In [22], the fractional part of the total delay is considered for further assessment in the RPCC. Based on the plant extended state-space model, a modified Luenberger observer with complete state feedback is designed to improve the system robustness. However, these RPCCs still suffer from steady-state current errors due to the disturbance caused by parameter mismatch and other unmodeled dynamics. In [23], an adaptive RPCC is presented to eliminate this current error, but an extra current error correction term increases the difficulty of system design and adjustment.

In this paper, the RPCC with online disturbance estimation is proposed for IM drives. The contributions of the proposed controller are: 1) the two-sample deadbeat control achieves fast current response; 2) the control with online disturbance estimation overcomes the weakness of a steady-state current error of the conventional RPCC.

The outline of this paper is as follows. In Section II, the IM mathematical model with disturbance is first given. Then, this model is improved with consideration of the control timing sequence. In Section III, the RPCC with disturbance estimation is proposed in a discrete-time domain, followed by stability analyses of the discrete Luenberger observer. In Section IV, the proposed scheme is analyzed in detail from the perspectives of static-errorless current control, stability, and dynamic performance. The experimental results verify the effectiveness of the proposed scheme in Section V.

II. System Descriptions

A. Modeling of IM With Uncertainties

In synchronous rotating *dq* reference frame, the IFOC-based IM mathematical model [24] is described as

$$\begin{cases} \dfrac{di_{sd}}{dt} = -\dfrac{R_s L_r^2 + R_r L_m^2}{\sigma L_s L_r^2} i_{sd} + \omega_e i_{sq} \\ \qquad + \dfrac{L_m R_r}{\sigma L_s L_r^2}\lambda_r + \dfrac{u_{sd}}{\sigma L_s} \\ \dfrac{di_{sq}}{dt} = -\dfrac{R_s L_r^2 + R_r L_m^2}{\sigma L_s L_r^2} i_{sq} - \omega_e i_{sd} \\ \qquad - \dfrac{L_m}{\sigma L_s L_r}\omega_r \lambda_r + \dfrac{u_{sq}}{\sigma L_s}. \end{cases} \tag{1}$$

For clarity, (1) can be expressed in matrix form

$$\frac{d\boldsymbol{i}}{dt} = \boldsymbol{A}\boldsymbol{i} + \boldsymbol{B}(\boldsymbol{u} - \boldsymbol{d}) \tag{2}$$

where

$$\boldsymbol{A} = -a_1\boldsymbol{I} + a_2\boldsymbol{J}, \boldsymbol{B} = b_1\boldsymbol{I}, \boldsymbol{I} = \begin{pmatrix} 1 & 0 \\ 0 & 1 \end{pmatrix}, \boldsymbol{J} = \begin{pmatrix} 0 & 1 \\ -1 & 0 \end{pmatrix}$$

$$a_1 = \frac{R_s L_r^2 + R_r L_m^2}{\sigma L_s L_r^2}, a_2 = \omega_e, b_1 = \frac{1}{\sigma L_s}$$

$$d_{sd} = -\frac{L_m R_r}{L_r^2}\lambda_r, d_{sq} = \frac{L_m}{L_r}\omega_r \lambda_r.$$

However, the IM parameters (resistances and inductances) cannot remain constant during runtime. Besides, the unmodeled dynamics further increase the model error. Taking all these disturbances into consideration, the IM model given in (2) is rewritten as

$$\begin{aligned} \frac{d\boldsymbol{i}}{dt} &= (\boldsymbol{A} + \Delta\boldsymbol{A})\boldsymbol{i} + (\boldsymbol{B} + \Delta\boldsymbol{B})[\boldsymbol{u} - (\boldsymbol{d} + \Delta\boldsymbol{d}) + \boldsymbol{\varepsilon}] \\ &= \boldsymbol{A}\boldsymbol{i} + \boldsymbol{B}(\boldsymbol{u} - \boldsymbol{d} - \boldsymbol{f}) \end{aligned} \tag{3}$$

where

$$\boldsymbol{f} = -\boldsymbol{B}^{-1}[\Delta\boldsymbol{A}\boldsymbol{i} + \Delta\boldsymbol{B}(\boldsymbol{u} - \boldsymbol{d} - \Delta\boldsymbol{d} + \boldsymbol{\varepsilon})] + \Delta\boldsymbol{d} - \boldsymbol{\varepsilon}.$$

If the sampling period T_s is selected short enough that the rotation angular during T_s can be neglected, we obtain the discrete-time form of (3) by applying the first-order Taylor expansion

$$\boldsymbol{i}(k+1) = (\boldsymbol{I} + \boldsymbol{A}T_s)\boldsymbol{i}(k) + \boldsymbol{B}T_s[\boldsymbol{u}(k) - \boldsymbol{d}(k) - \boldsymbol{f}(k)]. \tag{4}$$

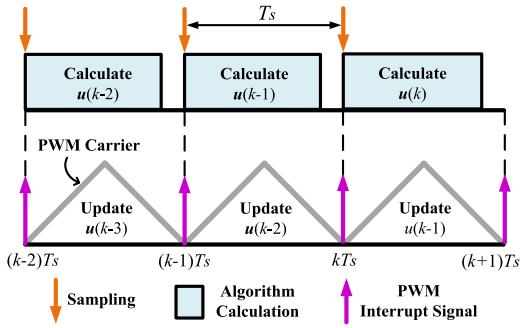

Fig. 1. Control timing sequence of the current loop.

B. Control Timing Sequence

In an industrial microprocessor-based control system, the sampling, algorithm calculation, and PWM update cannot be accomplished in the same instant [16], [17]. Thus, the impact of control delay has to be considered in controller design.

Fig. 1 shows the control timing sequence of the current loop. The sampling is set to synchronize with the PWM interrupt signal. Its advantage is that the sensed phase currents are close to the averaged current without switching noise [25], [26], which prevents measurement drift and lag caused by applying a current filter. Since the symmetrical PWM strategy is applied, a sampling period T_s before PWM interrupt signal is needed to finish the sampling and algorithm calculation. Supposing the delayed $\boldsymbol{i}'(t) \equiv \boldsymbol{i}(t - T_s)$, we get that $\boldsymbol{i}'(t)$ lags time T_s behind $\boldsymbol{i}(t)$. Thus, considering the control delay, the discrete-time model of IM shown in (4) becomes

$$\begin{aligned} \boldsymbol{i}'(k+1) &= (\boldsymbol{I} + \boldsymbol{A}T_s)\boldsymbol{i}'(k) \\ &\quad + \boldsymbol{B}T_s[\boldsymbol{u}(k-1) - \boldsymbol{d}(k-1) - \boldsymbol{f}(k-1)]. \end{aligned} \tag{5}$$

C. IM Drive System

Fig. 2 shows the block diagram of IFOC-based IM drive with the proposed current controller. A rectifier and inverter set which is controlled by the control unit is applied to drive the IM. The overall algorithm in the control unit adopts the commonly used cascade double closed-loop structure, including the speed loop

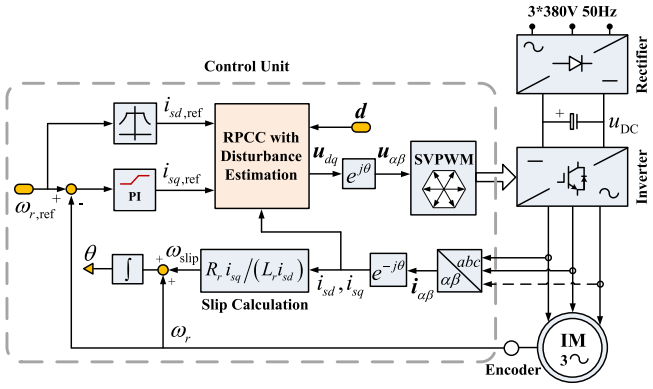

Fig. 2. Block diagram of IFOC-based IM drive with the proposed current controller.

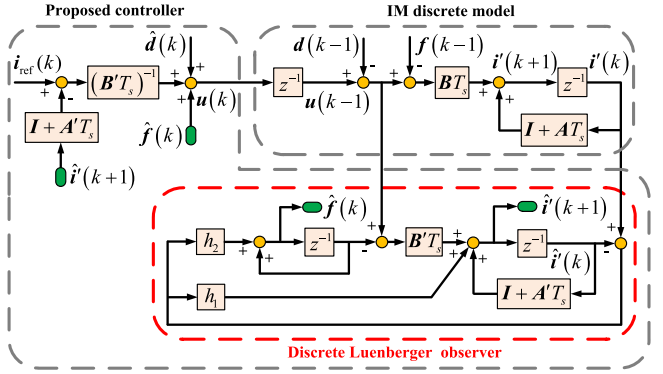

Fig. 3. Block diagram of a control system using the proposed RPCC with disturbance estimation in discrete-time domain.

(outer loop) and the current loop (inner loop). A PI-type controller is used for the speed loop control, and the proposed RPCC with disturbance estimation is applied for the current-loop control. The mechanical speed of IM is measured by an incremental encoder. The rotor position θ used for coordinate transformations is attained by integrating the synchronous angular speed ω_e.

III. Proposed RPCC With Disturbance Estimation

A. Design of RPCC With Disturbance Estimation

The RPCC with disturbance estimation is proposed to achieve fast current response in this section. By using a PWM interrupt period advanced of (5) and setting $\boldsymbol{i}'(k+2) = \boldsymbol{i}_{\mathrm{ref}}(k)$, we can get the command voltage $\boldsymbol{u}(k)$ of a two-sample deadbeat

$$\boldsymbol{u}(k) = \frac{\boldsymbol{i}_{\mathrm{ref}}(k) - \boldsymbol{i}'(k+1)}{\boldsymbol{B}'T_s} - \frac{\boldsymbol{A}'}{\boldsymbol{B}'}\boldsymbol{i}'(k+1) + \boldsymbol{d}(k) + \boldsymbol{f}(k) \tag{6}$$

where $\boldsymbol{A}'$ and $\boldsymbol{B}'$ are the control matrices with the measured IM parameters. When the measured values are consistent with the actual values, there are $\boldsymbol{A}' = \boldsymbol{A}$ and $\boldsymbol{B}' = \boldsymbol{B}$. In practical applications, $\boldsymbol{A}'$ and $\boldsymbol{B}'$ remain constant during runtime, while the actual IM parameters vary with time. It can be seen from (6) that $\boldsymbol{i}'(k+1)$, $\boldsymbol{d}(k)$, and $\boldsymbol{f}(k)$ are unknown variables during period kT_s to $(k+1)T_s$. Thus, we have to predict these unknown variables in period kT_s to $(k+1)T_s$.

First, a discrete Luenberger observer is proposed to predict $\boldsymbol{i}'(k+1)$ and $\boldsymbol{f}(k)$. According to (5) and assuming that the value of disturbance is constant during period kT_s to $(k+1)T_s$ [13], the IM discrete-time model can be written by taking the disturbance term as extended state

$$\begin{bmatrix} \boldsymbol{i}'(k+1) \\ \boldsymbol{f}(k) \end{bmatrix} = \begin{bmatrix} \boldsymbol{I} + \boldsymbol{A}'T_s & -\boldsymbol{B}'T_s \\ 0 & \boldsymbol{I} \end{bmatrix} \begin{bmatrix} \boldsymbol{i}'(k) \\ \boldsymbol{f}(k-1) \end{bmatrix} + \begin{bmatrix} \boldsymbol{B}'T_s \\ 0 \end{bmatrix} [\boldsymbol{u}(k-1) - \boldsymbol{d}(k-1)]. \tag{7}$$

On the basis of (7), the discrete Luenberger observer is designed as

$$\begin{bmatrix} \hat{\boldsymbol{i}}'(k+1) \\ \hat{\boldsymbol{f}}(k) \end{bmatrix} = \begin{bmatrix} \boldsymbol{I} + \boldsymbol{A}'T_s & -\boldsymbol{B}'T_s \\ 0 & \boldsymbol{I} \end{bmatrix} \begin{bmatrix} \hat{\boldsymbol{i}}'(k) \\ \hat{\boldsymbol{f}}(k-1) \end{bmatrix} + \begin{bmatrix} \boldsymbol{B}'T_s \\ 0 \end{bmatrix} [\boldsymbol{u}(k-1) - \boldsymbol{d}(k-1)] + \boldsymbol{H}\left(\begin{bmatrix} \boldsymbol{i}'(k) \\ \boldsymbol{i}'(k) \end{bmatrix} - \begin{bmatrix} \hat{\boldsymbol{i}}'(k) \\ \hat{\boldsymbol{i}}'(k) \end{bmatrix} \right) \tag{8}$$

where $\mathbf{H} = \begin{bmatrix} h_1\boldsymbol{I} & 0 \\ 0 & h_2\boldsymbol{I} \end{bmatrix}$ is the observer gain. Notice that the conventional RPCC [20], [21] is a particular case for $h_2 = 0$. By applying the Luenberger-type observer, (8) has the natural dynamic characteristics of IM, which means that the estimates can approach the actual variables under the same input. The stability of the proposed observer is detailed analyzed in Section III-B.

Second, the back EMF $\boldsymbol{d}(k)$ can be regarded as a slow time-varying variable in (6) [21]. Thus, assuming that the variation of $\boldsymbol{d}(k)$ over the switching period is linear, we can predict $\boldsymbol{d}(k)$ as

$$\hat{\boldsymbol{d}}(k) \approx 2\boldsymbol{d}(k-1) - \boldsymbol{d}(k-2). \tag{9}$$

Finally, replacing $\boldsymbol{i}'(k+1)$, $\boldsymbol{d}(k)$, and $\boldsymbol{f}(k)$ in (6) with their estimates calculated by (8) and (9) results in

$$\boldsymbol{u}(k) = \frac{\boldsymbol{i}_{\mathrm{ref}}(k) - \hat{\boldsymbol{i}}'(k+1)}{\boldsymbol{B}'T_s} - \frac{\boldsymbol{A}'}{\boldsymbol{B}'}\hat{\boldsymbol{i}}'(k+1) + \hat{\boldsymbol{d}}(k) + \hat{\boldsymbol{f}}(k). \tag{10}$$

Fig. 3 shows the block diagram of the control system using the proposed controller in discrete-time domain. The detailed analysis of the proposed controller is shown in Section IV.

TABLE I
JURY TABLE

	z^0	z^1	z^2
1	p_0	p_1	p_2

B. Stability Analysis of the Proposed Luenberger Observer

For simplification of analysis, we first apply the complex space vector theorem [24] in (8), which leads to

$$\begin{bmatrix} \hat{i}'_{dq}(k+1) \\ \hat{f}_{dq}(k) \end{bmatrix} = \begin{bmatrix} 1-a'_1T_s-a_2T_sj & -b'_1T_s \\ 0 & 1 \end{bmatrix} \begin{bmatrix} \hat{i}'_{dq}(k) \\ \hat{f}_{dq}(k-1) \end{bmatrix} + \begin{bmatrix} b'_1T_s \\ 0 \end{bmatrix} [u_{dq}(k-1) - d_{dq}(k-1)] + \begin{bmatrix} h_1 & 0 \\ 0 & h_2 \end{bmatrix} \begin{bmatrix} i'_{dq}(k) - \hat{i}'_{dq}(k) \\ i'_{dq}(k) - \hat{i}'_{dq}(k) \end{bmatrix} \tag{11}$$

where $i'_{dq} = i_{\mathrm{d}} + ji_q$ and $f_{dq} = f_d + jf_q$ are complex variables. When the PWM interrupt frequency is above 5 kHz, the small cross-coupling term $-a_2T_sj$ in (11) can be ignored in most cases ($a_2T_s = \omega_{\mathrm{e}}T_s < 0.01$ for $\omega_{\mathrm{e}} < 50$ Hz). Based on this, the observer characteristic equation is derived as

$$\begin{aligned} \Delta_o(z) &= \det\left(z\boldsymbol{I} - \begin{bmatrix} 1-a'_1T_s-h_1 & -b'_1T_s \\ -h_2 & 1 \end{bmatrix} \right) \\ &= p_2z^2 + p_1z + p_0 = 0 \end{aligned} \tag{12}$$

where $p_0 = 1 - a'_1T_s - h_1 - h_2b'_1T_s, p_1 = a'_1T_s + h_1 - 2$, $p_2 = 1$. Applying Jury criterion [27], we can obtain the Jury Table as shown in Table I. Then, the necessary and sufficient conditions for the observer stability is

$$\begin{cases} \Delta_o(1) = p_2 + p_1 + p_0 > 0 \\ (-1)^2\Delta_o(-1) = p_2 - p_1 + p_0 > 0 \\ |p_0| < p_2 \end{cases}. \tag{13}$$

Substituting the values of p_0, p_1, and p_2 in (12) into (13) yields

$$\begin{cases} -h_2b'_1T_s > 0 \\ 4 - 2a'_1T_s - 2h_1 - h_2b'_1T_s > 0 \\ 0 < a'_1T_s + h_1 + h_2b'_1T_s < 2 \end{cases}. \tag{14}$$

To satisfy (14), conditions (15) is obtained

$$\begin{cases} -a'_1T_s - h_2b'_1T_s < h_1 < 2 - a'_1T_s - \dfrac{h_2b'_1T_s}{2} \\ h_2 < 0 \end{cases}. \tag{15}$$

Therefore, to guarantee the stability of the proposed observer, the selection of h_1 and h_2 should satisfy conditions (15). In addition, the stability and dynamic performance of the proposed controller further limit the value ranges of h_1 and h_2, which will be analyzed in Section IV-B.

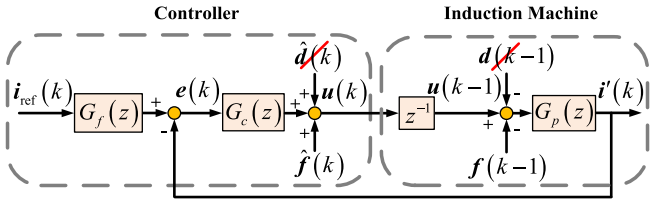

Fig. 4. Equivalent unity-feedback system in discrete-time domain.

IV. Analysis of the Proposed RPCC With Disturbance Estimation

In this section, the proposed controller will be compared with the conventional RPCC to show its improvements. Besides, the stability and dynamic performance of the proposed scheme is analyzed further. Considering that the conventional RPCC is a particular case for $h_2 = 0$ in (8), both the two controllers can be simplified as an equivalent unity-feedback system (see Fig. 4). The simplified controller is rearranged into two parts: the equivalent filter

$$G_f(z) = \boldsymbol{h'}^{-1}(\boldsymbol{I} + \boldsymbol{A'}T_s)^{-1}\left[\boldsymbol{I} - (\boldsymbol{I} + \boldsymbol{A'}T_s - \boldsymbol{h'})z^{-1}\right] \tag{16}$$

where $\boldsymbol{h'} = h_1\boldsymbol{I} - (h_2\boldsymbol{B'}T_s)/(z-1)$; and the controller

$$G_c(z) = z\boldsymbol{h'}(\boldsymbol{I} + \boldsymbol{A'}T_s)(\boldsymbol{B'}T_s)^{-1}(z\boldsymbol{I} + \boldsymbol{h'})^{-1}. \tag{17}$$

The IM is reformulated in discrete transfer function

$$G_p(z) = \boldsymbol{B}T_s[z\boldsymbol{I} - (\boldsymbol{I} + \boldsymbol{A}T_s)]^{-1}. \tag{18}$$

Notice that the estimated back EMF $\hat{\boldsymbol{d}}(k)$ is a feedforward term to the controller. Thus, $\boldsymbol{d}(k-1)$ on the machine side can be cancelled by $\hat{\boldsymbol{d}}(k)$ with consideration of the control delay z^{-1}[21], which excludes the impact of back-EMF variations.

A. Static-Errorless Current Control

First, the weakness of the steady-state current error of the conventional RPCC is analyzed. Applying $h_2 = 0$ in (8), we obtain $\hat{\boldsymbol{f}}(k) = 0$ in the conventional RPCC, and, thus, the disturbance term $\boldsymbol{f}(k-1)$ on the machine side cannot be canceled. According to Fig. 4, the error transfer function from $\boldsymbol{f}(k-1)$ to $\boldsymbol{e}(k)$ is calculated as

$$\Phi_e(z) = \frac{\boldsymbol{e}(z)}{\boldsymbol{f}(z)} = \frac{G_p(z)}{1 + G_c(z)z^{-1}G_p(z)}. \tag{19}$$

Based on the final-value theorem, the system steady-state error is obtained as

$$\boldsymbol{e}(\infty) = \lim_{z\to 1}\frac{z\boldsymbol{I} - \boldsymbol{I}}{z\boldsymbol{I}}\Phi_e(z)\boldsymbol{f}(z). \tag{20}$$

Assuming that the disturbance term is unit step-function signal $\boldsymbol{f}(t) = \boldsymbol{I}(t)$, then we get $\boldsymbol{f}(z) = \frac{z\boldsymbol{I}}{z\boldsymbol{I}-\boldsymbol{I}}$. Substituting $\boldsymbol{f}(z)$ and (19) into (20) yields

$$\boldsymbol{e}(\infty) = \frac{(1+h_1)\boldsymbol{B}T_s}{h_1\boldsymbol{I} - \boldsymbol{A}T_s}. \tag{21}$$

Therefore, due to the disturbance on the machine side, there is steady-state current error in the conventional RPCC.

Second, the proposed RPCC with disturbance estimation is analyzed for comparison. Applying $h_2 \neq 0$ in (8), we get $\hat{\boldsymbol{f}}(k) \neq 0$. Based on Fig. 4, we can obtain the steady-state error of the proposed scheme considering both $\boldsymbol{f}(k-1)$ and $\hat{\boldsymbol{f}}(k)$

$$\boldsymbol{e}'(\infty) = \lim_{z\to 1}\left(\frac{z\boldsymbol{I}-\boldsymbol{I}}{z\boldsymbol{I}}\Phi_e(z)\boldsymbol{f}(z) + \frac{z\boldsymbol{I}-\boldsymbol{I}}{z\boldsymbol{I}}\Phi_e{}'(z)\hat{\boldsymbol{f}}(z)\right) \tag{22}$$

where $\Phi_e'(z) = \frac{\boldsymbol{e}(z)}{\hat{\boldsymbol{f}}(z)} = -\frac{z^{-1}G_p(z)}{1+G_c(z)z^{-1}G_p(z)}$ is the error transfer function from $\hat{\boldsymbol{f}}(k)$ to $\boldsymbol{e}(k)$. Assuming that $\hat{\boldsymbol{f}}(k)$ can converge to its actual value in finite PWM interrupt periods, we get $\boldsymbol{f}(z) = z^{-1}\hat{\boldsymbol{f}}(z)$ by considering the control delay z^{-1}. Based on this assumption, substituting (19), $\Phi_e'(z)$ and $\boldsymbol{f}(z)$ into (22) yields

$$\boldsymbol{e}'(\infty) = \lim_{z\to 1}\left(\frac{z\boldsymbol{I}-\boldsymbol{I}}{z\boldsymbol{I}}\frac{G_p(z)}{1+G_c(z)z^{-1}G_p(z)}z^{-1}\hat{\boldsymbol{f}}(z) - \frac{z\boldsymbol{I}-\boldsymbol{I}}{z\boldsymbol{I}}\frac{G_p(z)z^{-1}}{1+G_c(z)z^{-1}G_p(z)}\hat{\boldsymbol{f}}(z)\right) = 0. \tag{23}$$

Thus, compared with the conventional RPCC, the proposed scheme fundamentally eliminates the steady-state current error by using the online disturbance estimation and correction.

B. Stability and Dynamic Performance of the Proposed Method

Based on Fig. 4, the open-loop transfer function of the equivalent unity-feedback system without filter is

$$H(z) = G_c z^{-1} G_p. \tag{24}$$

The closed-loop transfer function is

$$F(z) = \frac{G_f H(z)}{\boldsymbol{I}+H(z)}. \tag{25}$$

Assuming that the control error caused by machine parameter mismatch is compensated by the proposed method, we get $\boldsymbol{A}' \approx \boldsymbol{A}$ and $\boldsymbol{B}' \approx \boldsymbol{B}$. Then, substituting (16)–(18) and (24) into (25), we obtain

$$F(z) = \frac{G_f G_c z^{-1} G_p}{\boldsymbol{I}+G_c z^{-1} G_p} = z^{-2}. \tag{26}$$

Thus, the proposed controller is a two-sample deadbeat control with any observer gain $\boldsymbol{H}$. To further analyze the stability of the proposed controller, the characteristic equation of (26) is derived as

$$\Delta_c(z) = \boldsymbol{I} + G_c z^{-1} G_p = \left[\left(z^2-z\right)\boldsymbol{I} + \boldsymbol{h}'\right] \times \left[z\boldsymbol{I} - (\boldsymbol{I}+\boldsymbol{A}'T_s)\right] + \boldsymbol{h}'(z-1)(\boldsymbol{I}+\boldsymbol{A}'T_s) = 0. \tag{27}$$

Applying the complex space vector theorem [24] and ignoring the small cross-coupling term, we rewrite (27) as

$$\Delta_c(z) = \left[z^2 - (1-h_1)z - h_1 - h_2 b'_1 T_s\right](z-1+a'_1 T_s) + (zh_1 - h_1 - h_2 b'_1 T_s)(1-a'_1 T_s) = z\Delta_o(z) = 0. \tag{28}$$

TABLE II
PARAMETERS OF THE IM

Symbol	Quantity	Value
P_N	rated power	3.7 kW
V_N	rated voltage	380 V
ω_N	rated speed	1500 r/min
T_N	rated torque	23.6 N·m
n_p	number of pole pair	2
R_s	stator resistance	1.142 Ω
R_r	rotor resistance	0.825 Ω
L_m	mutual inductance	118.9 mH
L_s, L_r	stator, rotor inductance	124.4 mH
J_{tot}	total inertia	0.0256 kg·m^2

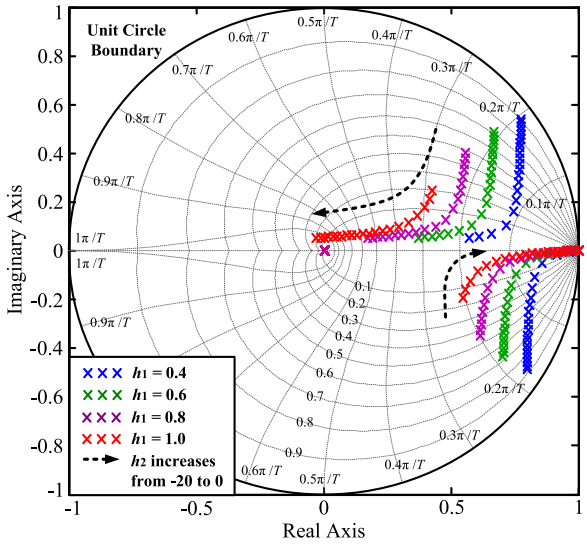

Fig. 5. Poles migration of the proposed controller with h_1 varied between 0.4 and 1, and h_2 varied between -20 and 0.

Compared (28) with (12), we find that the proposed controller has the same characteristic roots with the Lunberger observer except one more root in $z=0$. Therefore, the conditions (15) are also the necessary and sufficient conditions to guarantee the stability of the proposed controller. According to the IM parameters shown in Table II, the value range of h_1 and h_2 is selected as (29) to satisfy conditions (15):

$$\begin{cases} 0.4 \le h_1 \le 1 \\ -20 \le h_2 \le 0 \end{cases}. \tag{29}$$

To further verify the stability of the proposed controller with the selected h_1 and h_2 in (29), Fig. 5 describes the poles migration of (27) with h_1 varied between 0.4 and 1, and h_2 varied between -20 and 0. It can be seen that all the poles locate inside the unit circle, which means that the proposed controller is stable.

Moreover, the Bode plots are adopted to analyze the dynamic response and robustness of the proposed controller. Applying the bilinear transform in (24) yields

$$H(w) = G_c z^{-1} G_p\big|_{z=[1+(T/2)w]/[1-(T/2)w]}. \tag{30}$$

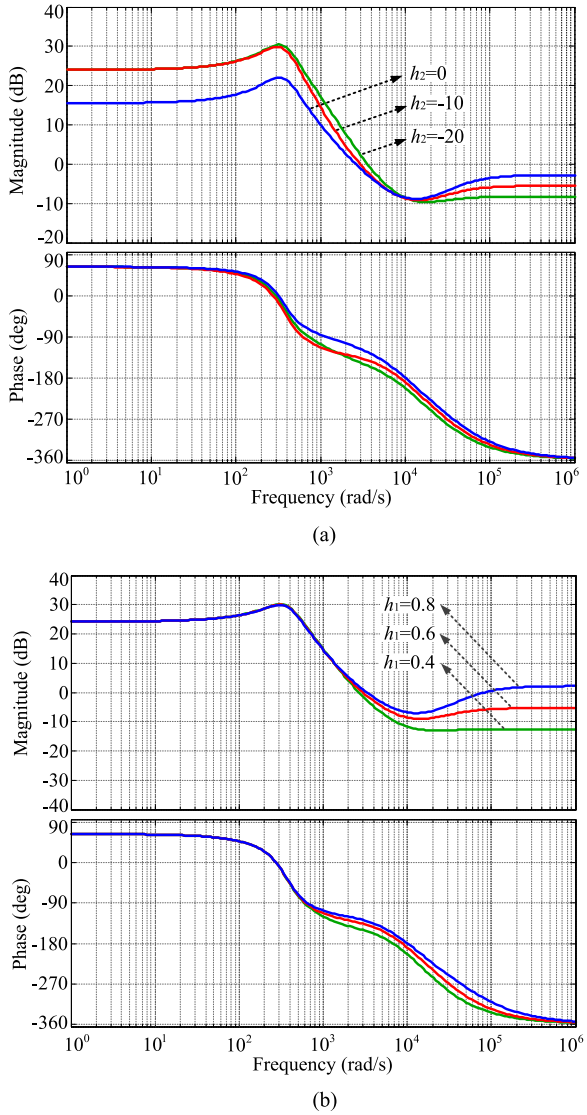

Fig. 6. Bode plots of the proposed RPCC with disturbance estimation. (a) $h_1 = 0.6, h_2$ varied between -20 and 0, step size of $h_2 = 10$ and (b) $h_2 = -10, h_1$ varied between 0.4 and 0.8, step size of $h_1 = 0.2$.

Fig. 6(a) shows the Bode plots of (30) with $h_1 = 0.6, h_2$ varied between -20 and 0. With the increase of h_2, the system cross-over frequency decreases, and likewise, the closed-loop bandwidth decreases, but at the same time, the system gain and phase margins increase accordingly. So there exists a tradeoff between the dynamic response and stability margin.

Fig. 6(b) is the Bode plots of (30) with $h_2 = -10, h_1$ varied between 0.4 and 0.8. As h_1 increases, the cross-over frequency changes slightly, while the gain and phase margins increase to some extent. Thus, the stability of the proposed controller can be enhanced by selecting larger h_1. However, excessive h_1 leads to high gain in high-frequency region, which indicates that the system reduced its robustness to high-frequency interference.

Given all these above, the observer gain are selected as $h_1 = 0.6, h_2 = -10$ here, which not only assures the stability, but balances the dynamic response and robustness of the proposed controller. By applying the selected h_1 and h_2 in (30), we obtain that the system cross-over frequency is 2.94×10^3 rad/s, and the gain and phase margins are 8.11 dB and 45°, respectively.

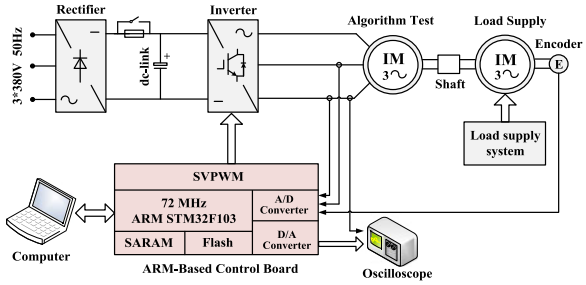

Fig. 7. Block diagram of the test bench.

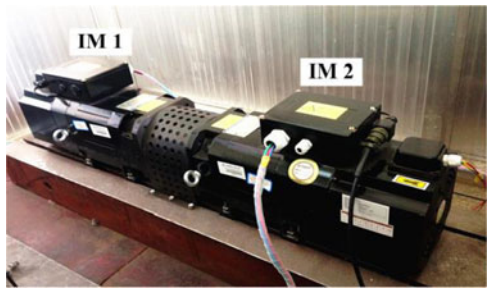

Fig. 8. Photograph of the IMs.

V. Experimental Results

The discussed method has been assessed experimentally on a test bench (see Fig. 7). The test setup is composed of:

1) Two IMs of the same model and rating (see Fig. 8), with parameters given in Table II. One is used for testing the proposed algorithm, while the other one is controlled by the load supply system.
2) *A rectifier and inverter set:* The rectifier rectifies the input alternating current into the direct current for the dc link, while the inverter provides the alternating current for the IM drive.
3) *An ARM-based control board:* A STM32F103 ARM serves as the control core. The ARM is a 32-bit fixed-point microcontroller with 72 MHz of maximum operating frequency, 128 kB of on-chip flash, and 20 kB of SRAM. Two-phase currents are measured for control. High-speed A/D and D/A converters are used for data conversion. The SVPWM is used to generate the inverter switching signals. A linked computer realizes the proposed algorithm and downloads the program to the ARM through an online emulator. An oscilloscope monitors the control variables.

The IFOC (see Fig. 2) is used as the basic control scheme. The reference values of i_{sd} and i_{sq} are set by using synchronous rotating reference frame. The symmetrical PWM strategy is used, where the PWM switching frequency is 6 kHz. The PWM interrupt period is 166.7 μs to provide adequate execution time for the essential algorithms. The gains of the proposed Luenberger observer are selected as $h_1 = 0.6$ and $h_2 = -10$.

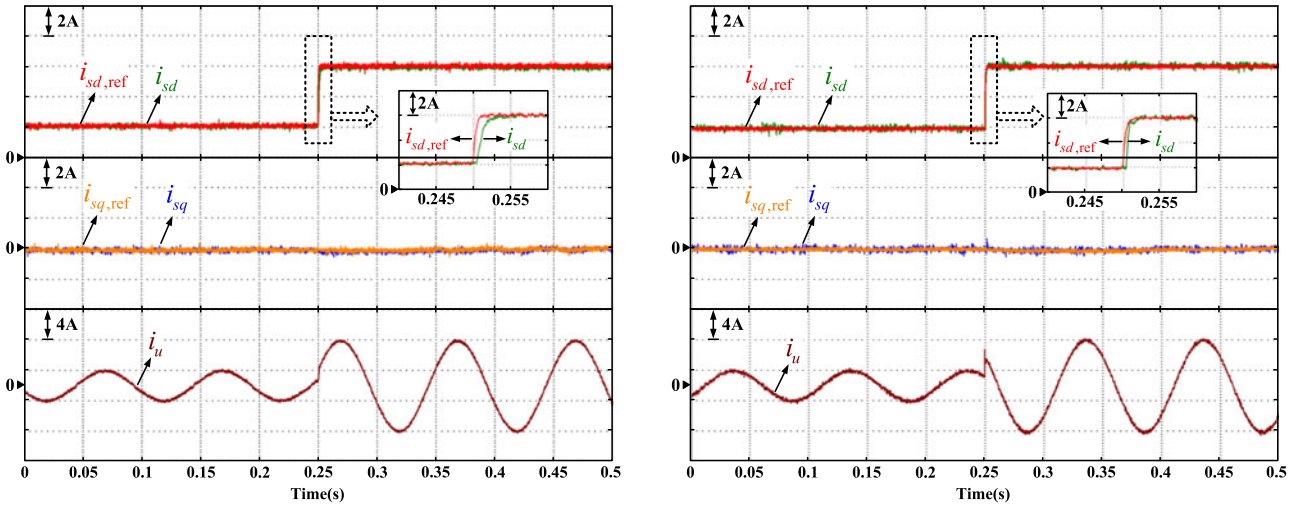

Fig. 9. Comparisons of the two controllers against step change of i_{sd} in the amplitude from 2 to 6 A. (a) Conventional PI controller and (b) proposed RPCC with disturbance estimation.

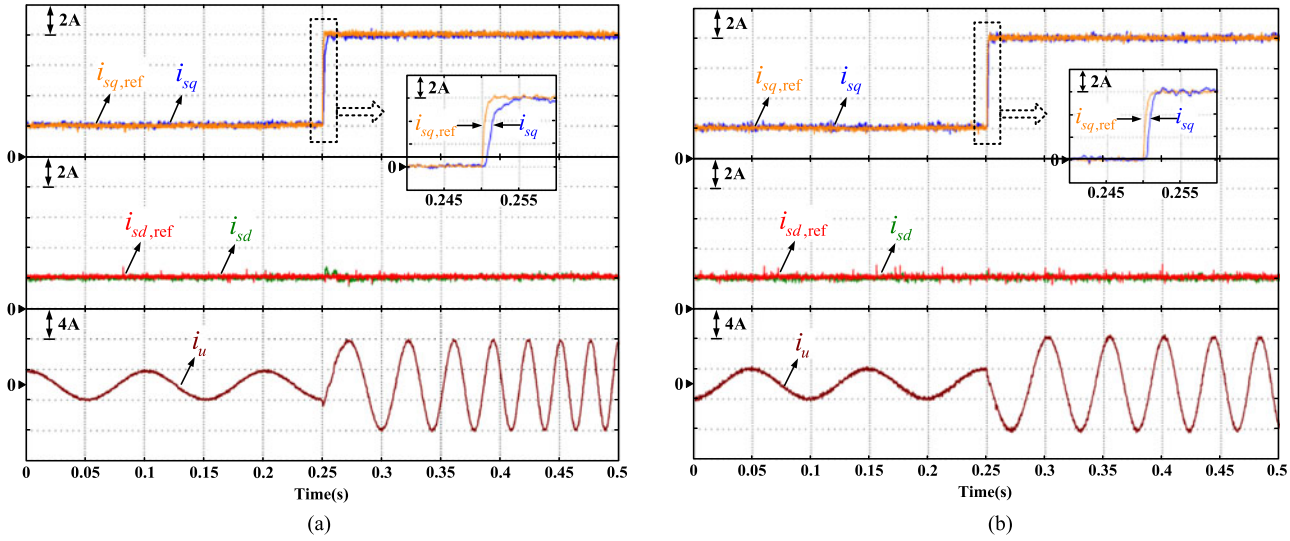

Fig. 10. Comparisons of the two controllers against step change of i_{sq} in the amplitude from 0 to 6 A. (a) Conventional PI controller and (b) proposed RPCC with disturbance estimation.

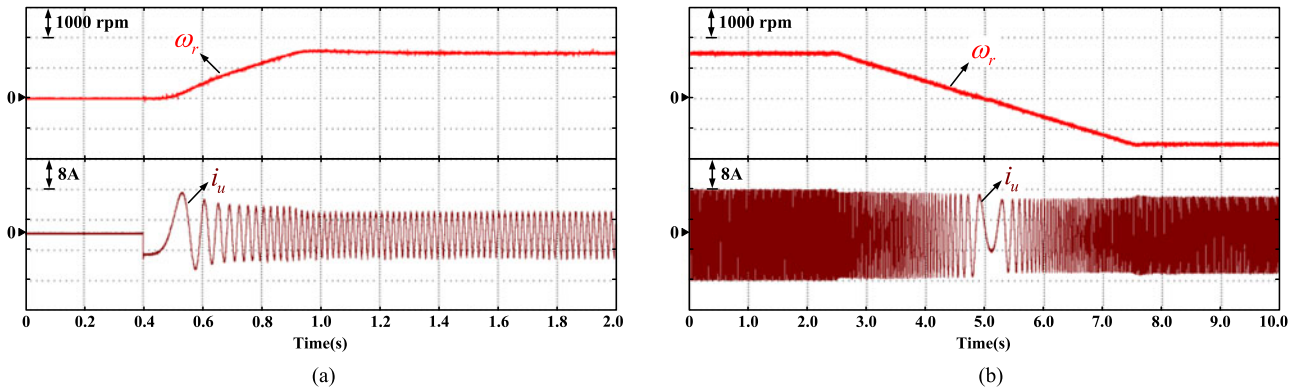

Fig. 11. Response of the proposed RPCC with disturbance estimation during speed increase and speed reversal. (a) Speed increase from 0 to rated speed, no load and (b) speed reversal at rated speed, rated load

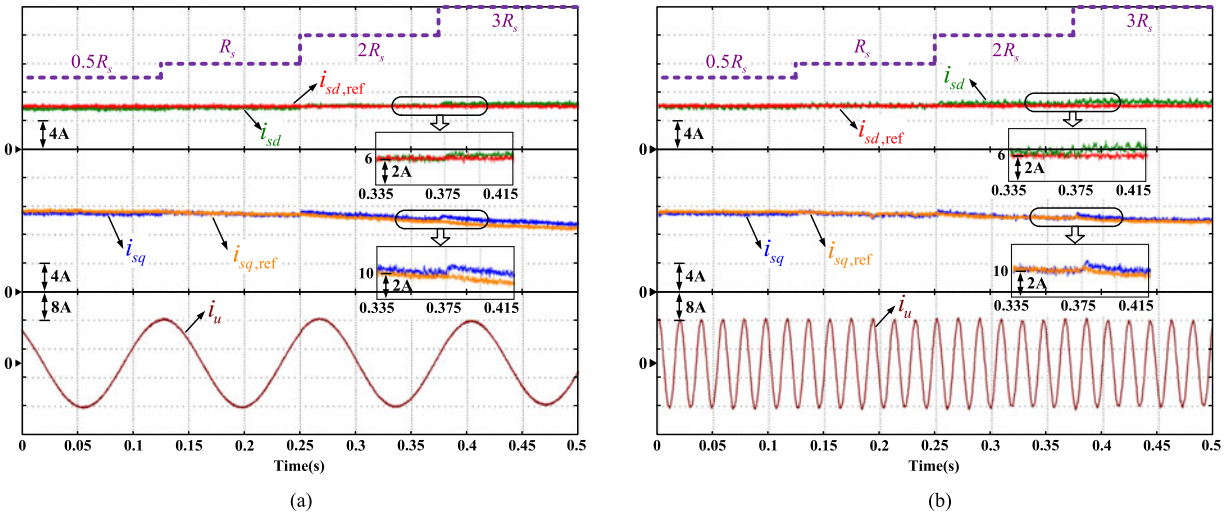

Fig. 12. Response of the conventional RPCC under R_s parameter mismatch.(a) 150 r/min, rated load, (b) 1500 r/min, rated load.

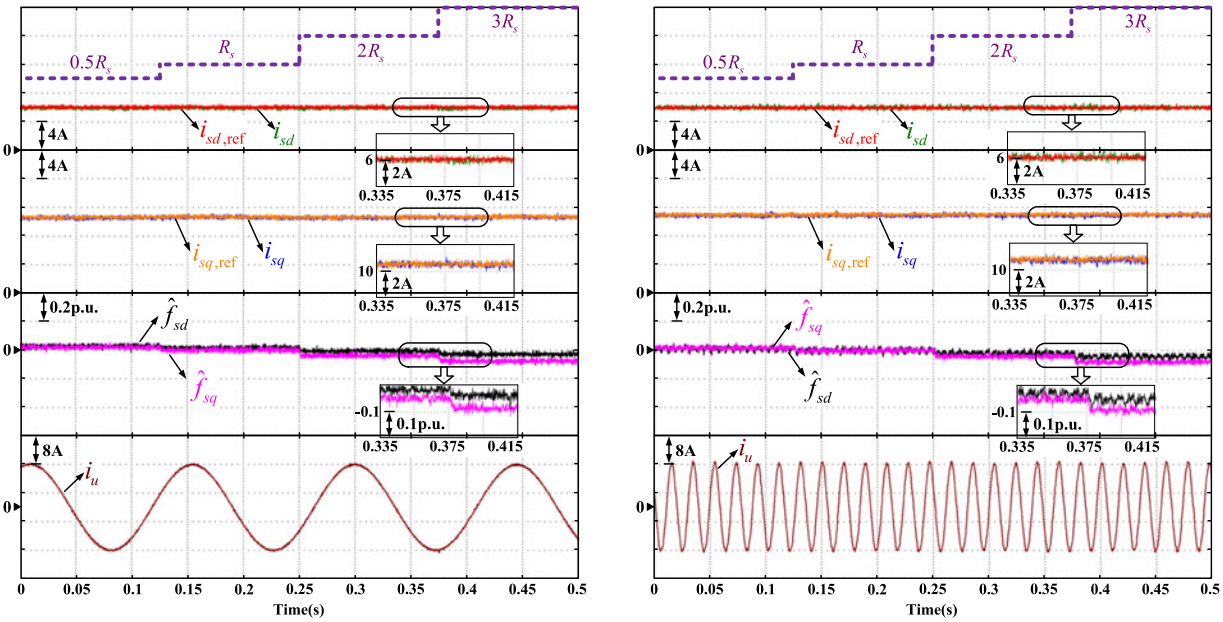

Fig. 13. Response of the proposed RPCC with disturbance estimation under R_s parameter mismatch. (a) 150 r/min rated load and (b) 1500 r/min, rated load.

A. *Dynamic Performance Tests*

First, as shown in Figs. 9 and 10, the dynamic performance of the proposed scheme is directly compared with that of the conventional PI controller [7], [28] under the same conditions. Each figure shows i_{sd}, i_{sq} and their reference $i_{sd,\mathrm{ref}}$, $i_{sq,\mathrm{ref}}$; and phase current i_u from top to bottom. Considering the dynamic response and overshoot of the PI controller, the proportional gain K_p and the integral coefficient K_i are selected as 13.5 and 0.40, respectively.

Fig. 9 shows the comparison of the two controllers against step change of $i_{sd,\mathrm{ref}}$ in the amplitude from 2 to 6 A at 300 r/min. Both controllers achieve accurate tracking of i_{sd} and i_{sq} without overshoot and steady-state error. However, the settling time of the proposed scheme is obviously shorter than that of PI controller, which means that the dynamic response of the proposed scheme is faster than that of PI controller.

Fig. 10 is the comparison of the two controllers against step change of $i_{sq,\mathrm{ref}}$ in the amplitude from 0 to 6 A. From 0 to 0.25 s, the machine is in speed close-loop control mode at 300 r/min. At 0.25 s, the speed loop is removed, and $i_{sq,\mathrm{ref}}$ is set to 6 A. Thus the machine begins to speed up. As expected, the settling time of the proposed scheme is shorter than that of the PI controller during step change of $i_{sq,\mathrm{ref}}$, which further demonstrates the superiority of the proposed scheme.

Second, as shown in Fig. 11, the experiments of speed increase and speed reversal are performed to show the overall performance of the proposed scheme. Fig. 11(a) is the response of the speed increase from 0 to rated value under no-load state,

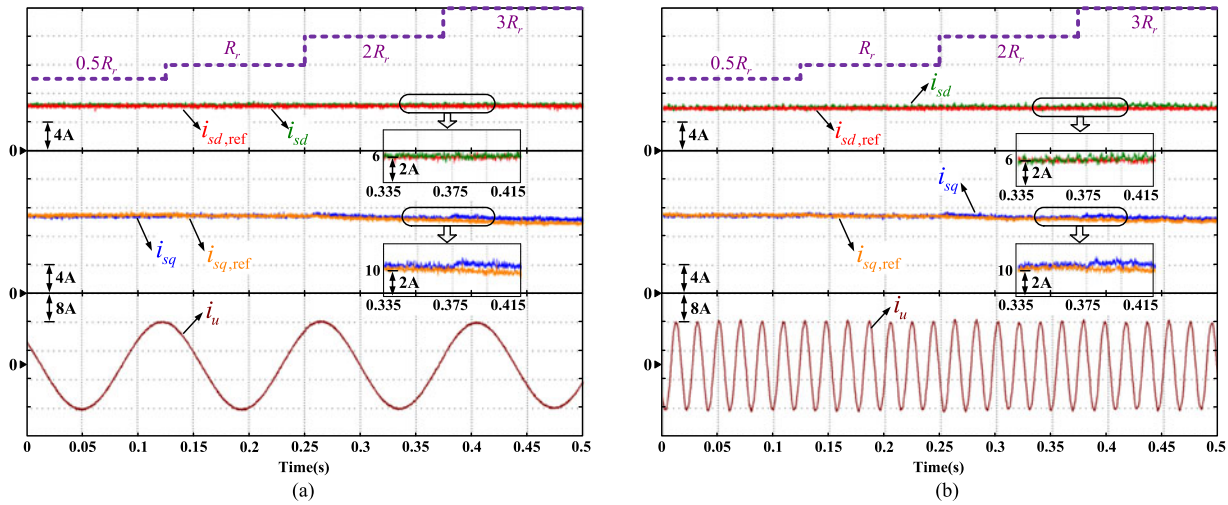

Fig. 14. Response of the conventional RPCC under R_r parameter mismatch. (a) 150 r/min, rated load and (b) 1500 r/min, rated load.

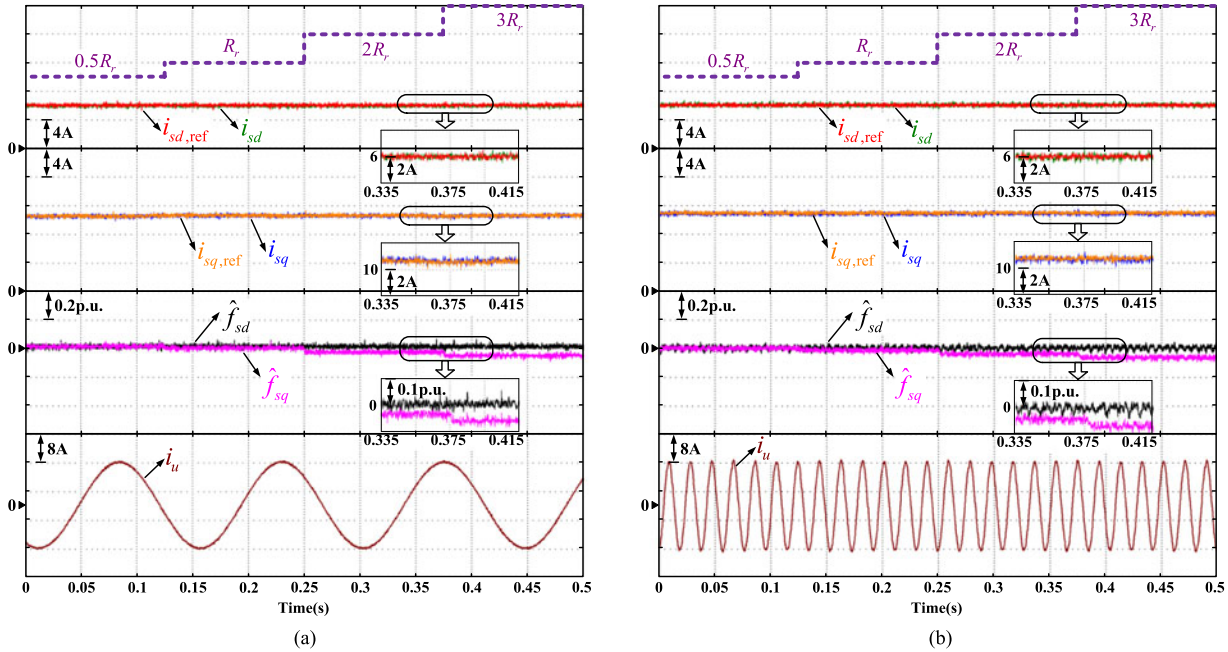

Fig. 15. Response of the proposed RPCC with disturbance estimation under R_r parameter mismatch. (a) 150 r/min, rated load and (b) 1500 r/min, rated load.

and Fig. 11(b) is the response of the speed reversal at rated speed under rated-load state. Notice that in Fig. 11(b), since the direction of load remains unchanged, the machine would turn from motoring state to regenerating state during the speed reversal. It can be seen from Fig. 11(a) and (b) that the machine operates stably and reliably by using the proposed scheme during the speed increase and the speed reversal.

B. Performance Tests Under Machine Parameter Mismatch

To verify the proposed scheme performance under machine parameter mismatch, Figs. 12 to 17 show the contrast results between the conventional RPCC [20] and the proposed scheme at both low speed (150 r/min) and high speed (1500 r/min). The stator resistance R_s, rotor resistance R_r, and mutual inductance L_m are chosen as the tested parameters. The sensitivity to each parameter variation is tested online with four step parameter changes: 50%, 100%, 200%, and 300% of the rated value. The way of the test is that the machine parameters are changed in the programming code of the current controller. The waveforms of i_{sd}, i_{sq} and their references $i_{sd,\mathrm{ref}}$, $i_{sq,\mathrm{ref}}$, and phase current i_u are separately given in each figure. Besides, the estimated disturbance terms $\hat{f}_{sd}$ and $\hat{f}_{sq}$ are also given in Figs. 13, 15, and 17.

Figs. 12 and 13 illustrate the responses of the conventional RPCC and the proposed scheme under R_s mismatch. In Fig. 12(a) and (b), i_{sd} and i_{sq}, especially i_{sq}, cannot accurately trace their references under R_s mismatch. Thus, the conventional RPCC is sensitive to R_s to some extent. In contrast, i_{sd} and i_{sq} accurately trace their references with the proposed

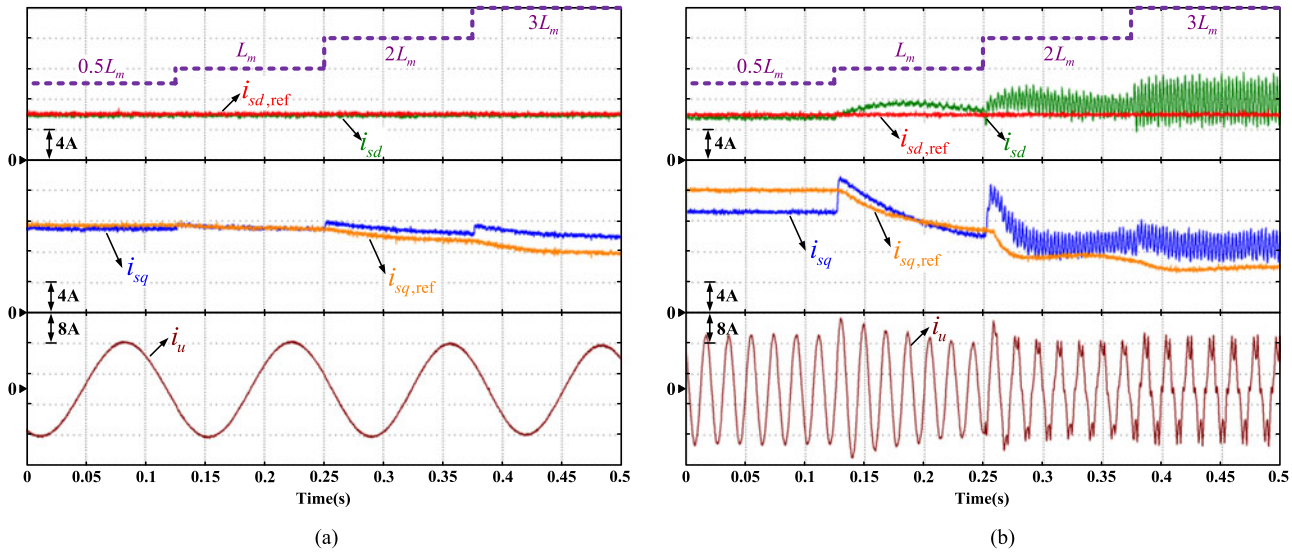

Fig. 16. Response of the conventional RPCC under L_m parameter mismatch. (a) 150 r/min, rated load and (b) 1500 r/min, rated load.

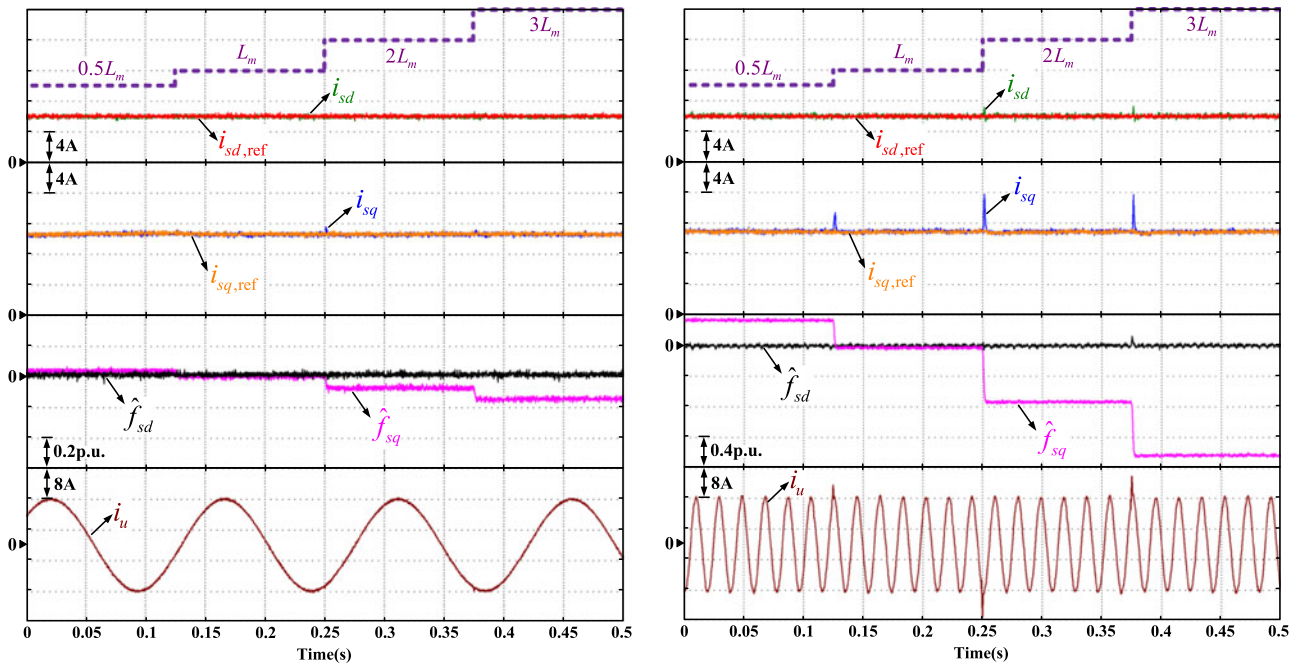

Fig. 17. Response of the proposed RPCC with disturbance estimation under L_m parameter mismatch. (a) 150 r/min, rated load and (b) 1500 r/min, rated load.

scheme in Fig. 13(a) and (b), where $\hat{f}_{sd}$ and $\hat{f}_{sq}$ compensate the steady-state current error caused by R_s mismatch.

Figs. 14 and 15 depict the responses of the conventional RPCC and the proposed scheme under R_r mismatch. Similar to Fig. 12(a) and (b), the i_{sq} in Fig. 14(a) and (b) cannot track its reference either. By contrast in Fig. 15(a) and (b), both i_{sd} and i_{sq} track their references accurately using the proposed scheme.

Figs. 16 and 17 are the responses of the conventional RPCC and the proposed scheme under L_m mismatch. As seen from Fig. 16(a) and (b), there exists significant current inaccuracies in the conventional RPCC. Especially at high speed (see Fig. 16(b)), when L_m is 50% of the rated value, i_{sq} is about 3.3 A smaller than its reference. When L_m increases to 200% of the rated value, the oscillation occurs in i_{sd} and i_{sq}, and the oscillation becomes more severe as L_m increases to 300% of the rated value. So the conventional RPCC is very sensitive to L_m. When the proposed scheme is applied (see Fig. 17(a) and (b)), the estimated $\hat{f}_{sd}$ and $\hat{f}_{sq}$ modify the current controller through feedforward compensation, which eliminates the current inaccuracies caused by L_m mismatch. Thus, i_{sd} and i_{sq} can quickly converge to their references with relatively

small fluctuations, and the static-errorless current control is achieved.

VI. Conclusion

The proposed RPCC with disturbance estimation can achieve fast current response, which is of significant importance for high-performance IFOC-based IM drives. The steady-state current tracking error caused by parameter variations and other unmodeled dynamics is eliminated by introducing the disturbance term into the proposed observer and control law. The appropriate selection of the observer gain can balance the dynamic response and robustness of the proposed controller.

The proposed scheme has been verified on an industrial IM drive. Compared with the commonly used PI controller, the proposed scheme shows its superiority in fast current response. In addition, the proposed scheme presents strong robustness in the case of resistances and inductance error ranging from 50% to 300% of the rated value, where the weakness of steady-state current error of the conventional RPCC is successfully overcome.

References

[1] B. Wu, *High Power Converters and AC Drives*. Piscataway, NJ, USA: IEEE Press, 2006.

[2] A. Consoli, G. Scarcella, and A. Testa, "Slip-frequency detection for indirect field-oriented control drives," *IEEE Trans. Ind. Appl.*, vol. 40, no. 1, pp. 194–201, Jan./Feb. 2004.

[3] L. Amezquita-Brooks, J. Liceaga-Castro, and E. Liceaga-Castro, "Speed and position controllers using indirect field-oriented control: A classical control approach," *IEEE Trans. Ind. Electron.*, vol. 61, no. 4, pp. 1928–1943, Apr. 2014.

[4] D. M. Stojic, M. Milinkovic, S. Veinovic, and I. Klasnic, "Stationary frame induction motor feed forward current controller with back EMF compensation," *IEEE Trans. Energy Convers.*, vol. 30, no. 4, pp. 1356–1366, Dec. 2015.

[5] R. Ramchand, K. Gopakumar, C. Patel, K. Sivakumar, A. Das, and H. Abu-Rub, "Online computation of hysteresis boundary for constant switching frequency current-error space-vector-based hysteresis controller for VSI-fed IM drives," *IEEE Trans. Power Electron.*, vol. 27, no. 3, pp. 1521–1529, Mar. 2012.

[6] M. P. Kazmierkowski and L. Malesani, "Current control techniques for three-phase voltage-source PWM converters: A survey," *IEEE Trans. Ind. Electron.*, vol. 45, no. 5, pp. 691–703, Oct. 1998.

[7] D. G. Holmes, B. P. McGrath, and S. G. Parker, "Current regulation strategies for vector-controlled induction motor drives," *IEEE Trans. Ind. Electron.*, vol. 59, no. 10, pp. 3680–3689, Oct. 2012.

[8] J. Holtz, J. Quan, J. Pontt, J. Rodríguez, P. Newman, and H. Miranda, "Design of fast and robust current regulators for high-power drives based on complex state variables," *IEEE Trans. Ind. Appl.*, vol. 40, no. 5, pp. 1388–1397, Sep./Oct. 2004.

[9] H. Abu-Rub, J. Guzinski, Z. Krzeminski, and H. Toliyat, "Predictive current control of voltage-source inverters," *IEEE Trans. Ind. Electron.*, vol. 51, no. 3, pp. 585–593, Jun. 2004.

[10] P. Cortes, M. Kazmierkowski, R. Kennel, D. Quevedo, and J. Rodriguez, "Predictive control in power electronics and drives," *IEEE Trans. Ind. Electron.*, vol. 55, no. 12, pp. 4312–4324, Dec. 2008.

[11] Y.-R. Mohamed and E. El-Saadany, "Robust high bandwidth discrete time predictive current control with predictive internal model—A unified approach for voltage-source PWM converters," *IEEE Trans. Power Electron.*, vol. 23, no. 1, pp. 126–136, Jan. 2008.

[12] L. Xu, D. Zhi, and W. B. Williams, "Predictive current control of doubly fed induction generators," *IEEE Trans. Ind. Electron.*, vol. 56, no. 10, pp. 4143–4153, Oct. 2009.

[13] C. Xia, M. Wang, Z. Song, and T. Liu, "Robust model predictive current control of three-phase voltage source PWM rectifier with online disturbance observation," *IEEE Trans. Ind. Informat.*, vol. 8, no. 3, pp. 459–471, Aug. 2012.

[14] J. Hu and Z. Zhu, "Improved voltage-vector sequences on dead-beat predictive direct power control of reversible three-phase grid-connected voltage-source converters," *IEEE Trans. Power Electron.*, vol. 28, no. 1, pp. 254–267, Jan. 2013.

[15] J. Guzinski and H. Abu-Rub, "Speed sensorless induction motor drive with predictive current controller," *IEEE Trans. Ind. Electron.*, vol. 60, no. 2, pp. 699–709, Jan. 2013.

[16] Q. Zeng and L. Chang, "An advanced SVPWM-based predictive current controller for three-phase inverters in distributed generation systems," *IEEE Trans. Ind. Electron.*, vol. 55, no. 3, pp. 1235–1246, Mar. 2008.

[17] J. Castello, J. M. Espi, and R. Garcia-Gil, "A new generalized robust predictive current control for grid-connected inverters compensates antialiasing filters delay," *IEEE Trans. Ind. Electron.*, vol. 63, no. 7, pp. 4485–4494, Jul. 2016.

[18] H.-T. Moon, H.-S. Kim, and M.-J. Youn, "A discrete-time predictive current control for PMSM," *IEEE Trans. Power Electron.*, vol. 18, no. 1, pp. 464–472, Jan. 2003.

[19] M. S. Zaky, M. M. Khater, S. S. Shokralla, and H. A. Yasin, "Wide speed-range estimation with online parameter identification schemes of sensorless induction motor drives," *IEEE Trans. Ind. Electron.*, vol. 56, no. 5, pp. 1699–1707, May 2009.

[20] J. C. Moreno, J. M. Espi Huerta, R. G. Gil, and S. A. Gonzalez, "A robust predictive current control for three-phase grid-connected inverters," *IEEE Trans. Ind. Electron.*, vol. 56, no. 6, pp. 1993–2004, Jun. 2009.

[21] J. M. Espi Huerta, J. Castello, J. R. Fischer, and R. Garcia-Gil, "A synchronous reference frame robust predictive current control for three-phase grid-connected inverters," *IEEE Trans. Ind. Electron.*, vol. 57, no. 3, pp. 954–962, Mar. 2010.

[22] J. R. Fischer, S. A. Gonzalez, M. A. Herran, M. G. Judewicz, and D. O. Carrica, "Calculation-delay tolerant predictive current controller for three-phase inverters," *IEEE Trans. Ind. Informat.*, vol. 10, no. 1, pp. 233–242, Feb. 2014.

[23] J. M. Espi, J. Castello, R. García-Gil, G. Garcera, and E. Figueres, "An adaptive robust predictive current control for three-phase grid-connected inverters," *IEEE Trans. Ind. Electron.*, vol. 58, no. 8, pp. 3537–3546, Aug. 2011.

[24] S. K. Sul, *Control of Electric Machine Drive Systems*. Hoboken, NJ, USA: Wiley, 2011, ch. 4.

[25] V. Blasko, V. Kaura, and W. Niewiadomski, "Sampling of discontinuous voltage and current signals in electrical drives: A system approach," *IEEE Trans. Ind. Appl.*, vol. 34, no. 5, pp. 1123–1130, Sep./Oct. 1998.

[26] S.-H. Song, J.-W. Choi, and S.-K. Sul, "Current measurements in digitally controlled ac drives," *IEEE Ind. Appl. Mag.*, vol. 6, no. 4, pp. 51–62, Jul./Aug. 2000.

[27] K. Ogata, *Discrete-Time Control Systems*. Englewood Cliffs, NJ, USA: Prentice-Hall, 1987, ch. 4.

[28] D.-C. Lee, S.-K. Sul, and M.-H. Park, "High performance current regulator for a field-oriented controlled induction motor drive," *IEEE Trans. Ind. Appl.*, vol. 23, no. 5, pp. 1247–1257, Sep./Oct. 1994.

Bo Wang (S'16) was born in Shandong Province, China, in 1987. He received the B.S. degree in electrical engineering from Northwestern Polytechnical University, Xi'an, China, in 2011, and the M.S. degree in electrical engineering from Harbin Institute of Technology, Harbin, China, in 2013, where he is currently working toward the Ph.D. degree in electrical engineering.

His research interests include induction machine drives and nonlinear control theories and applications.

Xianle Chen was born in Zhejiang Province, China, in 1992. She received the B.S. degree in electrical engineering from Harbin Institute of Technology, Weihai, China, in 2015. She is currently working toward the M.S. degree in electrical engineering at Harbin Institute of Technology, Harbin, China.

Her research interests include induction machine drives and applications.

Yong Yu was born in Jilin Province, China, in 1974. He received the B.S. degree in electromagnetic measurement and instrumentation in 1995 from Harbin Institute of Technology (HIT), Harbin, China, where he also received the M.S. and Ph.D. degrees in electrical engineering in 1997 and 2003, respectively.

From 2004 to 2014, he was an Associate Professor in the Department of Electrical Engineering, HIT, where he has been a Professor of electrical engineering since 2014. His current research interests include electrical motor drives, power quality mitigation, and fault diagnosis and tolerant control of inverter.

Gaolin Wang (M'13) received the B.S., M.S., and Ph.D. degrees in electrical engineering from Harbin Institute of Technology, Harbin, China, in 2002, 2004, and 2008, respectively.

From 2009 to 2012, he was a Postdoctoral Fellow with Shanghai STEP Electric Corporation. In 2009, he joined the Department of Electrical Engineering, Harbin Institute of Technology, as a Lecturer, where he has been a Professor of electrical engineering since 2014. He has authored more than 30 technical papers published in journals and conference proceedings. He is the holder of seven Chinese patents. His current major research interests include permanent magnet synchronous motor drives, high-performance direct-drive for traction system, position sensorless control of AC motors, and efficiency optimization control of interior PMSM.

Dianguo Xu (M'97–SM'12) received the B.S. degree in control engineering and the M.S. and Ph.D. degrees in electrical engineering from Harbin Engineering University (HIT), Harbin, China, in 1982, 1984, and 1989, respectively.

In 1984, he joined the Department of Electrical Engineering, HIT, as an Assistant Professor. Since 1994, he has been a Professor in the Department of Electrical Engineering, HIT. He was the Dean with the School of Electrical Engineering and Automation, HIT, from 2000 to 2010. He is currently the Vice President with HIT. He has published more than 600 technical papers. His research interests include renewable energy generation technology, power quality mitigation, sensorless vector controlled motor drives, and high-performance PMSM servo system.

Dr. Xu is an Associate Editor of the IEEE TRANSACTIONS ON INDUSTRIAL ELECTRONICS and the IEEE JOURNAL OF EMERGING AND SELECTED TOPICS IN POWER ELECTRONICS. He serves as the Chairman of the IEEE Harbin Section.